



Design of direct-formed square and rectangular hollow section stub columns

Kamran Tayyebi, Min Sun *

Department of Civil Engineering, University of Victoria, Victoria, British Columbia V8P 5C2, Canada



ARTICLE INFO

Article history:

Received 10 September 2020
Received in revised form 14 December 2020
Accepted 21 December 2020
Available online xxxx

Keywords:

Direct forming
Square hollow section
Rectangular hollow section
Stub column
Galvanizing
Finite element analysis
High-strength steel

ABSTRACT

Provisions in the current steel design standards do not differentiate square and rectangular hollow sections (SHS and RHS) members cold-formed by different approaches. Research on the effect of post-cold-forming hot-dip galvanizing on residual stress and stub column behaviour is also insufficient. Complementary experimental studies showed that: (1) the stub column behaviour of a direct-formed SHS/RHS (regular-strength or high-strength) is superior to its indirect-formed counterpart; (2) the current codified slenderness limits and the effective width method tend to misjudge a non-slender direct-formed section as a slender section, resulting in an unnecessary penalty and member strength underestimation; and (3) post-cold-forming galvanizing can effectively relieve residual stress and improve the stub column behaviour of a direct-formed SHS/RHS. This research presents a finite element (FE) study with models developed using previously measured residual stresses, strength properties and geometric imperfections in direct-formed SHS/RHS. The modelling approach was validated against previous experimental data from 24 stub column tests. The stub column behaviour of direct-formed regular- and high-strength SHS/RHS (untreated and galvanized) was studied via an FE parametric study, including 624 models to cover a wide range of cross-sectional dimensions and material properties. The relevant provisions in the current design standards were examined. The experimental and FE data justifies the use of higher design curves for direct-formed SHS/RHS (untreated and galvanized). Modifications to the existing design rules for SHS/RHS stub columns against cross-sectional yielding or local buckling were proposed.

© 2020 Elsevier Ltd. All rights reserved.

1. Introduction

Square and rectangular hollow sections (SHS and RHS) in North America are manufactured predominantly by two approaches:

(1) Indirect forming (Fig. 1a): cold-forming the coil material into a circular shape initially, followed by closing the section using electric resistance welding (ERW), and finally cold-shaping the circular shape into a square or rectangular shape.

(2) Direct-forming (Fig. 1b): cold-forming the coil material directly to a square or rectangular shape, and closing the section using ERW.

Recent investigations (e.g. [1–7]) have been conducted on indirect-formed SHS/RHS with nominal yield stresses from 460 to 1100 MPa. Literature reviews in [8,9] pointed out that dedicated research on the effects of direct forming and the post-production processes (e.g. galvanizing and heat treatment to different degrees) on member behaviour is still insufficient.

Design rules in the existing steel standards do not differentiate SHS/RHS members cold-formed by different approaches. Based on a comprehensive experimental research program [8,9] consisting of tensile coupon

tests, stub column tests, residual stress measurements and geometric imperfection measurements, it was found that direct-formed SHS/RHS (with nominal yield strengths of 350 MPa and 690 MPa) have superior stub column behaviour than their indirect-formed counterpart, primarily due to an inherently low level of residual stress.

In practice, by performing a heat treatment to a CSA G40.20/G40.21 Class H finish [10], or an ASTM A1085 Supplement S1 finish [11], a higher column curve in the Canadian steel design standard [12] can be used. Producers typically specify a 30-min holding time once the furnace temperature is stable at 450 °C or higher [13,14]. Such heat treatment can effectively relieve the residual stress from cold forming and improve the column behaviour. Since the direct forming approach only cold work the corners of an SHS/RHS cross-section, it was found by [8,9] that the stub column behaviour of direct-formed SHS/RHS can sometimes be comparable to indirect-formed and subsequently heat-treated sections. For a total of 12 untreated direct-formed RHS stub columns (with nominal yield strengths of 350 MPa and 690 MPa), the experimentally obtained capacities were compared to the nominal cross-sectional strengths calculated from CSA S16-19 [12], ANSI/AISC 360-10 [15], EN-

* Corresponding author.

E-mail address: msun@uvic.ca (M. Sun).

Nomenclature

B	Measured external width of RHS
b	Flat width of plate element
b_e	Effective width of plate element
C_1	Material coefficient
C_ϕ	Calibration coefficient for reliability analysis
E	Young's modulus
$E_{0.2}$	Tangent modulus of steel material at 0.2% proof stress
E_{sh}	Initial slope of strain hardening
F_m	Mean value of fabrication factor for reliability analysis
f_u	Ultimate stress
f_y	Yield stress
H	Measured external depth of RHS
m	Second strain hardening exponent
M_m	Mean value of material factor for reliability analysis
n	First strain hardening exponent
P_{cr1}	Elastic local buckling load in AISI S100-16
P_{FE}	Stub column strength from finite element analysis
P_m	Mean value of test/FEA-to-predicted load ratios for reliability analysis
P_n	Nominal compressive strength of stub column
P_{ne}	Nominal axial strength for overall buckling in AISI S100-16
P_{nl}	Nominal axial strength for local buckling in AISI S100-16
P_{test}	Experimental stub column strength
P_u	Stub column strength from test or FE analysis
P_y	Cross-section yield load of stub column
t	Wall thickness of SHS/RHS
V_F	Coefficient of variation of the fabrication factor for reliability analysis
V_M	Coefficient of variation of material factor for reliability analysis
V_P	Coefficient of variation of test/FE-to-predicted load ratios for reliability analysis
V_Q	Coefficient of variation of load effect for reliability analysis
α	Flat width-to-thickness ratio for the initial geometric imperfection model
β	Reliability index
δ	Measured magnitude of initial geometric imperfection
$\epsilon_{0.2}$	Strain at 0.2% proof stress
ϵ_{sh}	Strain at the onset of strain hardening
ϵ_u	Strain at ultimate stress
ϵ_y	Strain at yield stress
λ	Slenderness factor in modified direct strength method
λ_l	Slenderness factor in AISI S100-16
$\bar{\lambda}$	Normalized plate slenderness
$\bar{\lambda}_{lim}$	Normalized yield slenderness limit
$\sigma_{0.05}$	0.05% proof stress of material
σ_b	Magnitude of longitudinal bending residual stress
σ_{in}	Total through-thickness residual stress at the inside surface of SHS/RHS
σ_m	Longitudinal membrane residual stress
σ_{out}	Total through-thickness residual stress at the outside surface of SHS/RHS
ϕ	Resistance factor

1993-1-1 [16] and the Direct Strength Method (DSM) in AISI S100-16 [17]. In all cases, the code predictions were excessively conservative. In addition, according to a linear regression of the experimental data, the existing slenderness limits in [12,15,16] were proven to be overly conservative for high-strength direct-formed SHS/RHS. As a result, the

effective width method based on the existing slenderness limits caused significant strength underestimation due to unnecessary penalties on the effective cross-sectional area. In this research, a parametric study is performed using FE models that incorporated the measured residual stresses, strength properties and geometric imperfections from [8,9], and subsequently validated using the stub column test data in [8]. The aim is to generate sufficient data for accurate evaluations of the existing design rules, and if necessary, to propose modifications to the current design rules for SHS/RHS stub columns against cross-sectional yielding or local buckling.

In practice, hot-dip galvanizing of hollow section members of commonly specified sizes in a 450 °C molten zinc bath takes approximately 10 min. Based on a comprehensive comparison on a total of 36 stub columns with different production histories, it was also found in the complementary experimental studies by [8,9] that the effects of galvanizing and post-cold-forming heat treatment to 450 °C for a 30-min holding time per [10,11] were comparable. It was speculated that, for hollow section members of commonly specified sizes, hot-dip galvanizing could also effectively relieve residual stress and delay local buckling. In this research, this speculation is also examined via an FE parametric study.

2. Finite element analysis

2.1. Elements, meshing and boundary conditions

A literature survey was performed on previous FE research on tubular stub columns. The modelling approaches therein were found to be consistent. Therefore, in this study, the method used by [3] was followed. The finite element software package ABAQUS [18] was used to conduct the numerical simulation. A four-node shell element with reduced integration (S4R) from the ABAQUS element library was used to model the SHS/RHS stub columns. Based on a mesh sensitivity analysis, a mesh size of $(H + B)/25$ mm was selected for the FE analyses, where H and B are the external depth and the width of the SHS/RHS, respectively. All nodes at each end of the stub column were tied to a restrained rigid body reference point. The top end could freely move in the axial direction to allow the application of displacement increments to simulate the axial compression force.

2.2. Material properties

In this research, the SHS/RHS are given IDs with multiple components to differentiate material type, post-cold-forming process, and cross-sectional sizes. For the first component, D = direct-formed RHS (nominal yield stress = 350 MPa), and DH = direct-formed high-strength RHS (nominal yield stress = 690 MPa). For the second component, U = untreated, and G = galvanized. Where applicable, the third component gives the nominal width, depth, and thickness of the cross-section (in mm). Using the experimental data and the constitutive equations proposed by [19,20], the engineering stress-strain relationships were developed and subsequently converted to true stress-strain relationships for use in ABAQUS [18] for the parametric study.

As shown in Fig. 1b, cold working is concentrated at the corner regions of an SHS/RHS during direct forming. By testing tensile coupons machined from the flat faces of the untreated direct-formed SHS/RHS, clear yield plateaus and large proportional stress-over-yield stress ratios were observed. Typical flat face stress-strain curves of two untreated direct-formed RHS are shown in Fig. 2a. As also shown in [8], the proportional stress-over-yield stress ratios in the galvanized sections increased in all cases due to an effective residual stress reduction from the galvanizing process. Typical engineering stress-strain curves of the flat face materials of two galvanized direct-formed RHS are shown in Fig. 2b. In both figures, the curves are similar to those of hot-rolled steels. Therefore, for the flat face materials, the quad-linear model

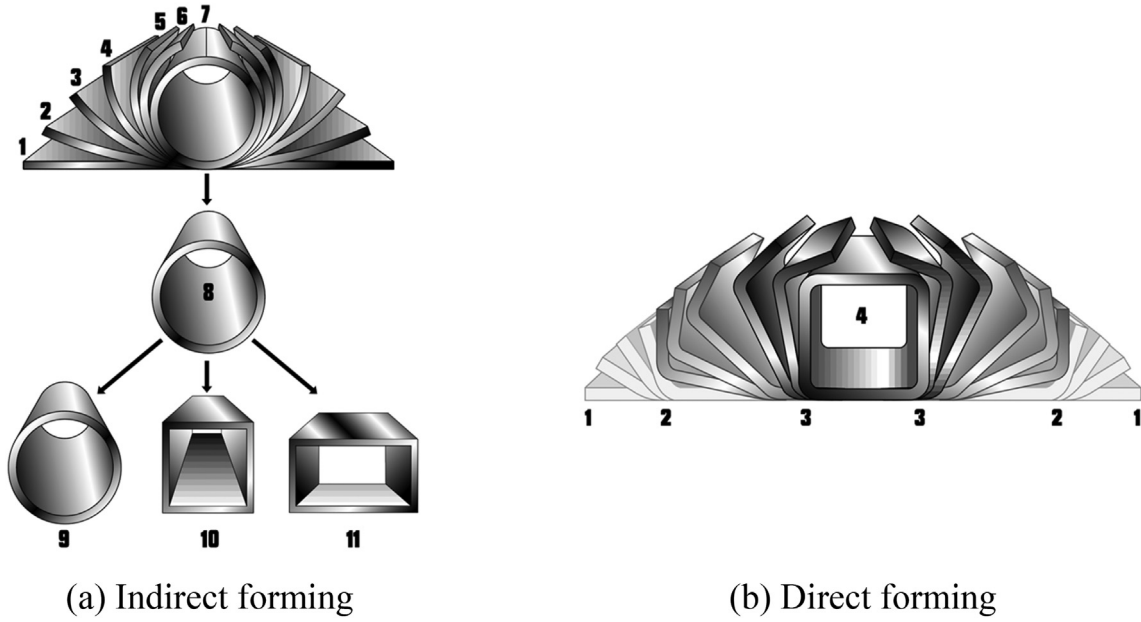


Fig. 1. Cold-forming approaches.

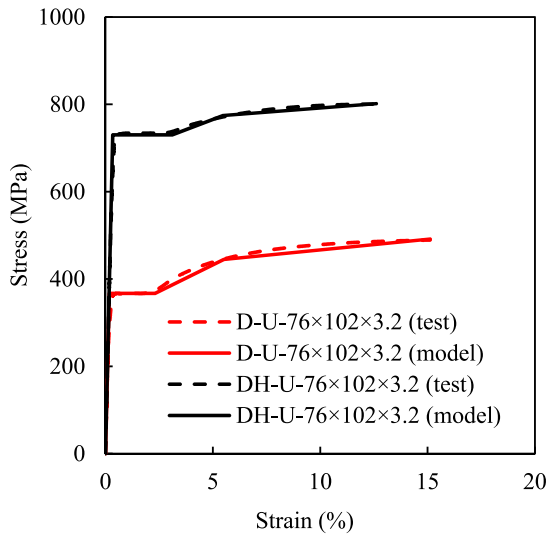
proposed by Yun and Gardner [19] for hot-rolled steels (reproduced as Eqs. (1)–(3) herein) was applied to simulate the stress-strain relationship in FE analysis. As shown in Fig. 2, Eqs. (1)–(3) can generate curves that fit well with the experimental data in all cases. The average values of the key material characteristics of the flat face tensile coupons from the untreated and the galvanized SHS/RHS (regular- and high-strength) in [8] were used in Eqs. (1)–(3) to generate the engineering stress-strain relationship (D-U-Flat, DH-U-Flat, D-G-Flat and DH-G-Flat). These values are listed in Table 1.

$$f(\varepsilon) = \begin{cases} E\varepsilon & \varepsilon < \varepsilon_y \\ f_y & \varepsilon_y < \varepsilon \leq \varepsilon_{sh} \\ f_y + E_{sh}(\varepsilon - \varepsilon_{sh}) & \varepsilon_{sh} < \varepsilon \leq C_1\varepsilon_u \\ f_{C_1\varepsilon_u} + \frac{f_u - f_{C_1\varepsilon_u}}{\varepsilon_u - C_1\varepsilon_u}(\varepsilon - C_1\varepsilon_u) & C_1\varepsilon_u < \varepsilon \leq \varepsilon_u \end{cases} \quad (1)$$

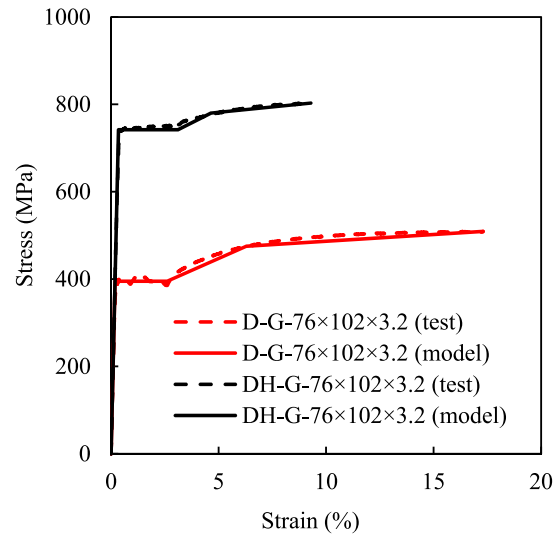
$$C_1 = \frac{\varepsilon_{sh} + 0.25(\varepsilon_u - \varepsilon_{sh})}{\varepsilon_u} \quad (2)$$

$$E_{sh} = \frac{f_u - f_y}{0.4(\varepsilon_u - \varepsilon_{sh})} \quad (3)$$

Different from the flat face materials, rounded tensile stress-strain curves were obtained in [8] for the corners of the untreated SHS/RHS due to cold working. Typical curves are shown in Fig. 3. The material model proposed by Gardner and Yun [20] for cold-formed steels (reproduced as Eqs. (4)–(7) herein) was applied to simulate the engineering stress-strain relationship. Fig. 3 shows that Eqs. (4)–(7) can generate curves that fit well with the experimental data in both cases. The average values of the key material characteristics of the corner tensile coupons from the untreated SHS/RHS (regular- and high-strength) in [8] were used in Eqs. (4)–



(a) Untreated RHS



(b) Galvanized RHS

Fig. 2. Typical engineering stress-strain curves of flat faces of untreated and galvanized RHS.

Table 1
Parameters for quad-linear stress-strain models.

Material ID	E (MPa)	f_y (MPa)	f_u (MPa)	ϵ_u	ϵ_y	ϵ_{sh}	E_{sh} (MPa)	C_1	$C_1\epsilon_u$	$f_{C1\epsilon_u}$ (MPa)
D-U-Flat	202,500	383	475	0.1621	0.0019	0.0258	1686	0.369	0.0599	444
DH-U-Flat	202,000	708	784	0.1184	0.0035	0.0244	2013	0.405	0.0479	754
D-G-Flat	206,400	421	490	0.1402	0.0020	0.0332	1617	0.428	0.0599	469
DH-G-Flat	204,200	732	792	0.1036	0.0036	0.0304	2056	0.470	0.0487	767
D-G-Corner	219,400	585	622	0.0577	0.0027	0.0218	2576	0.533	0.0308	604
DH-G-Corner	222,000	894	906	0.0531	0.0040	–	–	–	–	–

(7) to generate the engineering stress-strain relationships (D-U-Corner and DH-U-Corner). These characteristic values are listed in Table 2. The yield stress (f_y) in Table 2 was determined using the 0.2% proof stress method.

$$\epsilon = \begin{cases} \frac{f}{E} + 0.002 \left(\frac{f}{f_y} \right)^n & f \leq f_y \\ \frac{f-f_y}{E_{0.2}} + \left(\epsilon_u - \epsilon_{0.2} - \frac{f_u-f_y}{E_{0.2}} \right) \left(\frac{f-f_y}{f_u-f_y} \right)^m + \epsilon_{0.2} & f_y < f \leq f_u \end{cases} \quad (4)$$

$$n = \frac{\ln(4)}{\ln\left(\frac{f_y}{\sigma_{0.05}}\right)} \quad (5)$$

$$E_{0.2} = \frac{E}{1 + 0.002n \frac{E}{f_y}} \quad (6)$$

$$m = 1 + 1.33 \frac{f_y}{f_u} \quad (7)$$

As discussed earlier, previous research [8,9] found that for hollow section members of commonly specified sizes, hot-dip galvanizing can effectively relieve residual stresses. This observation was substantiated by comparing the corner coupon test results from the untreated and galvanized SHS/RHS specimens. In all cases, the stress-strain curves of the corner coupons from the galvanized SHS/RHS showed clear yield plateaus. Typical curves are shown in Fig. 4. Noticeable differences can be

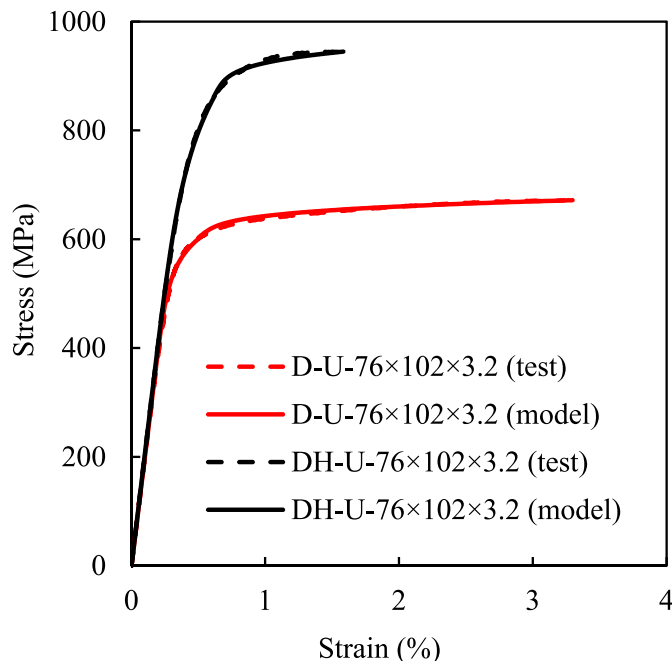


Fig. 3. Typical engineering stress-strain curves of corner regions of untreated RHS.

seen by comparing Figs. 3 and 4. Therefore, using the average key tensile coupon test results in Table 1, Eqs. (1)–(3) were applied to generate the engineering stress-strain relationships for the corner regions of the galvanized RHS (D-G-Corner and DH-G-Corner). For the corner regions of the galvanized high-strength SHS/RHS (DH-G-Corner in Table 1), the experimentally obtained stress-strain relationship was nearly bilinear (see Fig. 4). Such behaviour was modelled by assigning zero values to the strain hardening parameters in Eqs. (1)–(3).

The engineering stress-strain relationships developed using Eqs. (1)–(7) were subsequently converted to true stress-strain relationships for use in ABAQUS for the parametric study. Due to severe cold working, the materials at the corner and the adjacent regions, in general, have larger yield and ultimate stresses than the flat faces [6,8,9,21]. Similar to the approach used by [6,21], for FE modelling in this study, the experimentally obtained corner material properties were assigned to the corner regions and the adjacent regions (Fig. 5). [6] used an extended width of two times the wall thickness ($2t$). [21] used $1t$, $2t$ and $3t$, and found on average a 4% stub column strength difference. In this study, the extended corner regions have a width of $3t$ as the FE results match the experimental results the best in this case, which will be further discussed in the following sections.

2.3. Residual stresses

The inclusion of longitudinal residual stress in FE analysis is critical for simulation of steel members under axial compression [6,22]. In an earlier investigation complementary to this research, Tayyebi et al. [9] experimentally measured the longitudinal residual stresses in 26 SHS/RHS specimens with different production histories (indirect-formed, direct-formed, heat-treated, and galvanized) and with various material properties (nominal yield strengths of 350 and 690 MPa). The procedures suggested by [23–27] were adopted for the calculation of residual stresses. As shown in Fig. 6, the through-thickness residual stress was resolved into a membrane component and a bending component.

The average values of the normalized membrane and bending residual stresses in direct-formed SHS/RHS are listed in Table 3, where the tensile membrane residual stresses are reported as positive values, and the compressive membrane residual stresses are reported as negative values. The tabulated bending residual stresses are the tensile residual stresses from the external surfaces of the SHS/RHS specimens. It is evident in Table 3 that the current practice of post-cold-forming hot-dip galvanizing can effectively reduce residual stresses. Tayyebi and Sun [8] showed that post-cold-forming galvanizing can improve the stub column behaviour of cold-formed hollow sections. This study will implement the measured residual stresses in an FE parametric study to quantify such improvement over a wide range of cross-sectional sizes.

The approach suggested by [6,21] was adopted in this study to incorporate the measured residual stresses in the FE analyses in ABAQUS [18]. Five integration points were considered through the thickness of each element to ensure the accurate application of the residual stress distribution. Subroutine SIGINI was used to apply the stress magnitude at each integration point.

Table 2
Parameters for stress-strain models for corner regions of untreated RHS.

Material ID	E (MPa)	f_y (MPa)	f_u (MPa)	$\alpha_{0.05}$	ϵ_u	$\epsilon_{0.2}$	$E_{0.2}$ (MPa)	n	m
D-U-Corner	211,200	573	621	471	0.0174	0.0047	33,994	7.07	4.04
DH-U-Corner	203,400	862	950	700	0.0159	0.0062	48,997	6.68	3.99

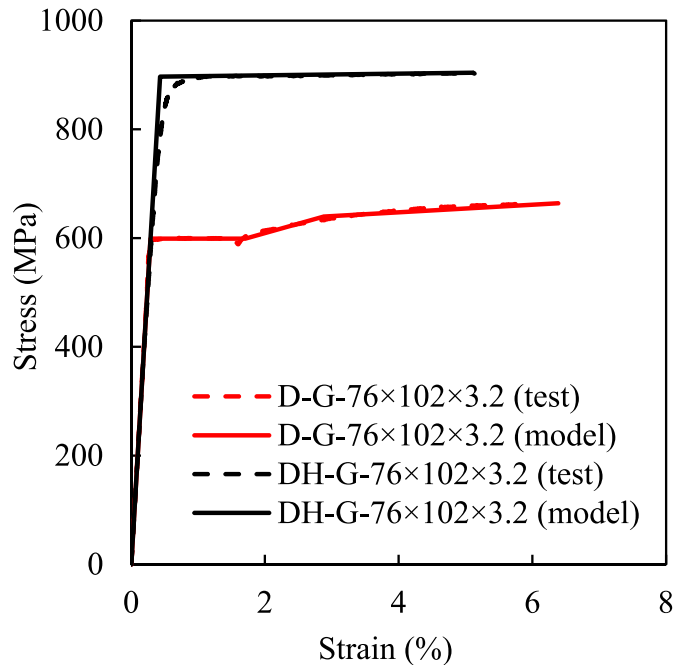


Fig. 4. Typical engineering stress-strain curves of corner regions of galvanized RHS.

For the corner region of the untreated SHS/RHS, rounded tensile stress-strain curves shown in Fig. 3 were obtained from tensile coupon tests (i.e. relatively small proportional limit-over-yield stress ratio due to the existence of bending residual stress) [3]. As discussed in Section 2.2, the tensile stress-strain relationship can be modelled

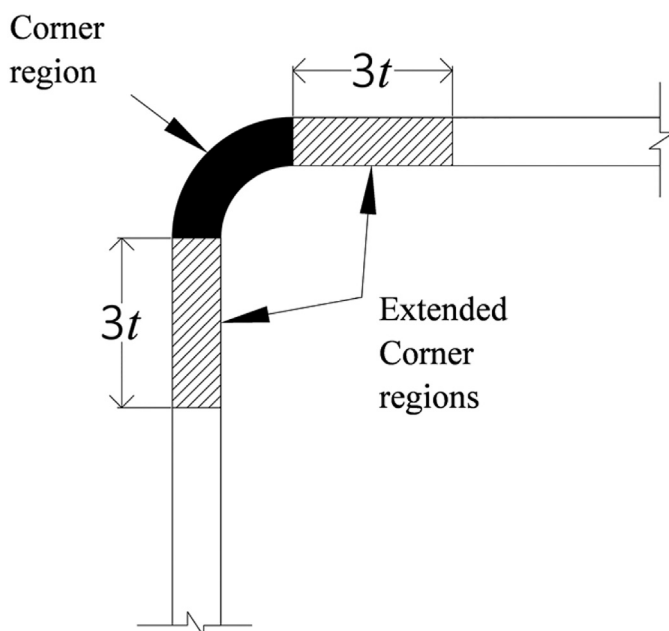


Fig. 5. Extension of corner material properties to adjacent flat faces.

accurately by Eqs. (4)–(7). Following the approach in [3,21], since the tensile coupons were clamped in the universal testing machine to the in-situ straight state before testing, the bending residual stresses were already included in the FE models by incorporating the rounded stress-strain curves. The membrane residual stresses were manually added to the FE models using the “initial conditions” function in ABAQUS.

As discussed in Section 2.2, although residual stresses were measured at the corner regions of galvanized SHS/RHS and the flat faces of all SHS/RHS [9], as shown in Figs. 2 and 4, the linear stress-strain relationship described by Eqs. (1)–(3) provided the best fit of the experimentally obtained stress-strain curves. However, the direct incorporation of such a relationship in FE modelling does not account for the bending residual stress. Therefore, for the corner regions of galvanized SHS/RHS and the flat faces of all SHS/RHS, both bending residual stresses and membrane residual stresses were added manually in the FE models.

Using the approaches in [6,21], as shown in Fig. 5, an extension of the corner region was considered to account for the cold forming effect. The measured residual stresses at corners were applied to the corner regions and the extended flat zones. The measured flat face residual stresses were added to the remaining areas of the cross-sections.

2.4. Initial geometric imperfections

Only local geometric imperfections are considered herein since this study is focused on the stub column behaviour. To include the effect of local geometric imperfections in FE analysis, the lowest eigenmode shape is typically chosen as the local geometric imperfection profile [3]. The maximum magnitude over the entire profile can be obtained from experimental measurements. For this numerical research, the geometric imperfections measured over four representative stub column specimens in the complementary study by Tayyebi and Sun [8] were adopted. The average values of the imperfections (δ) for the direct-formed regular- and high-strength RHS were 0.387 and 0.366 mm, respectively. By correlating the measured values to the SHS/RHS wall thicknesses (t), these correspond to 0.12 t and 0.08 t for the direct-formed regular- and high-strength SHS/RHS, respectively. On the other hand, Ma et al. [6] suggested that for FE analysis, the measured imperfections can be correlated to the width-to-thickness ratio of flat elements $\alpha = (B - 4t) / t$, where B is the external width. In this case, the average values obtained by Tayyebi and Sun [8] correspond to 0.014 α and 0.023 α for the direct-formed regular- and high-strength SHS/RHS, respectively. Since there is no unified rule for the correlation of initial imperfections to FE models, the larger value of the two different approaches was attempted in this study (i.e., 0.12 t and 0.023 α). The comparison is discussed in Section 2.5.

2.5. Verification of FE modelling

Results of the numerical models were verified against the 24 stub column test results from Tayyebi and Sun [8]. Comparisons of numerical analyses and experimental tests were made using representative load-displacement relationships and failure modes in Figs. 7 and 8. Tables 3 and 4 include the comparisons of ultimate loads from the stub column tests and FE analyses for the direct-formed regular- and high-strength SHS/RHS, respectively. In all cases, good agreements were observed. Therefore, credence was given to the accuracy of the FE modelling. As shown in Tables 4 and 5, the application of the two geometric

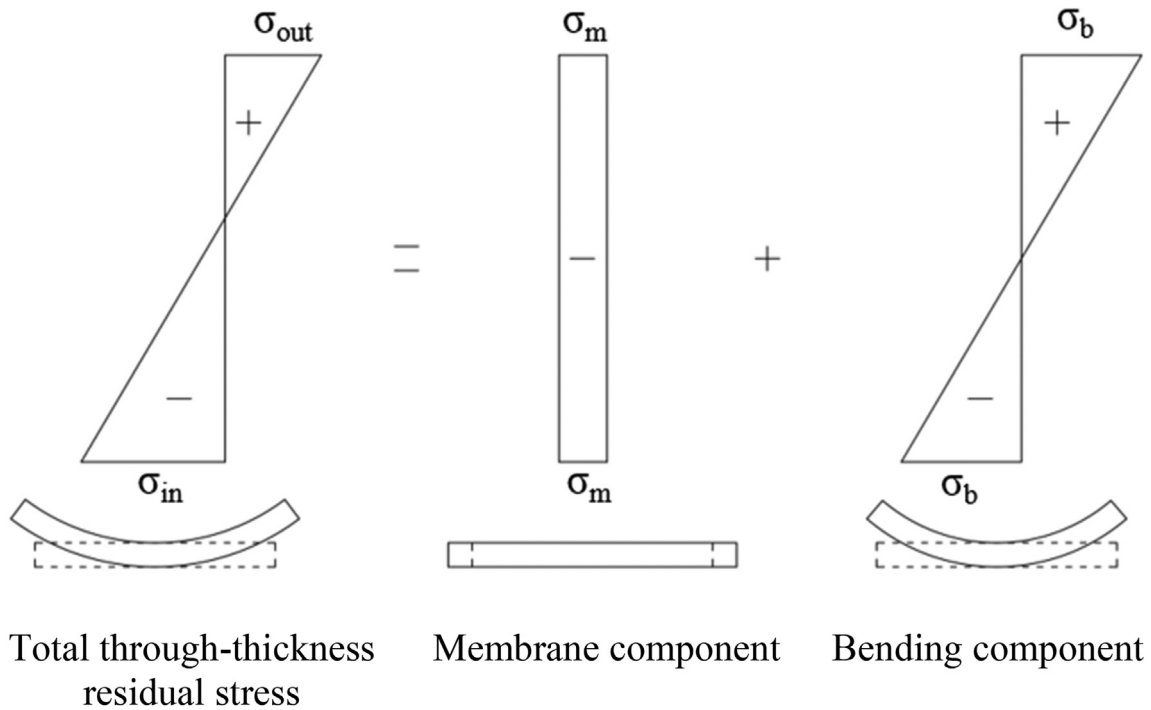


Fig. 6. Bending and membrane residual stress components.

Table 3
Average values of longitudinal residual stresses from [9].

Specimen ID	Center of flat face		Corner	
	Membrane	Bending	Membrane	Bending
D-U	$-0.06f_y$	$0.39f_y$	$0.08f_y$	$0.25f_y$
D-G	$-0.07f_y$	$0.27f_y$	$0.02f_y$	$0.14f_y$
DH-U	$-0.03f_y$	$0.50f_y$	$0.08f_y$	$0.22f_y$
DH-G	$-0.05f_y$	$0.29f_y$	$0.01f_y$	$0.13f_y$

imperfection modelling approaches (i.e., $0.12t$ and 0.023α) resulted in negligible differences. For the subsequent parametric study, a maximum local geometric imperfection of $0.12t$ was applied.

2.6. Parametric studies

The FE modelling approach verified in Section 2.5 was subsequently used to perform a parametric study, including a total of 624 stub column models (156 untreated SHS, 156 galvanized SHS, 156 untreated RHS, and 156 galvanized RHS). The 624 stub column models included 314 high-strength sections and 310 regular-strength sections. The material and residual stress properties in Sections 2.2 and 2.3 were used in the analyses. The width (and depth) of the sections ranged from 75 to 310 mm. The wall thickness varied from 2.5 to 13 mm. The cross-sectional width-to-depth ratio of the RHS ranged from 0.5 to 0.75. The selected dimensions cover the practical ranges of commonly available SHS/RHS products. The width-to-thickness (and depth-to-thickness) ratio ranged from 7 to 97. A length of three times the larger external dimension of the cross section was set as the stub column length, following the recommendations by the Structural Stability Research Council (SSRC) [28].

3. Stub column behaviours of SHS with different production histories

In this section, the experimental and FE data for the direct-formed SHS are compared to the indirect-formed SHS from [3,4,29,30], and to

the hot-finished SHS from [4,29,31], to study the effects of different production techniques. The comparison was made among sections with similar nominal yield strengths and cross-sectional dimensions. The effect of hot-dip galvanizing on the stub column behaviour of regular- and high-strength SHS was also studied.

The experimentally and numerically obtained ultimate loads (P_u) are normalized to the cross-sectional squash loads (P_y) in Figs. 9–12. The squash loads were calculated using the experimentally measured yield stress of the flat face material, which is consistent with the approach used in previous research [e.g. 4,6]. This is also consistent with the rationale for cross-section classification in existing design standards [e.g. 12,15,16], where the strength difference between the flat face and corner region is not considered.

Since the experimental data for indirect-formed and hot-finished SHS from [3,4,29–31] was only available for a certain range of plate slenderness, Figs. 9 and 10 only included the experimental and FE data for direct-formed SHS within the same range of plate slenderness for direct comparison. Since different design standards have different formulae for calculation of slenderness, following the approach adopted by [4,6], in this study a normalized plate slenderness ($\bar{\lambda}$) was calculated using Eq. (8). This also standardizes the evaluation of the slenderness limits in various design specifications, which will be further discussed in Section 4.

$$\bar{\lambda} = \frac{b\sqrt{f_y/E}}{t} \quad (8)$$

where b = internal width of SHS/RHS excluding corner portions, and E = Young's modulus.

In comparison to the untreated direct-formed SHS data in Fig. 9, the results of the indirect-formed SHS in Fig. 9 exhibit a relatively larger scatter. As shown in Fig. 9, the indirect-formed SHS in many cases have lower P_u/P_y -ratios due to the existence of high residual stresses, which subsequently lead to loss of stiffness and load-carrying capacities. To differentiate nonslender and slender cross sections, previous studies [e.g. 4,6] often involve linear regression of the available data. For the

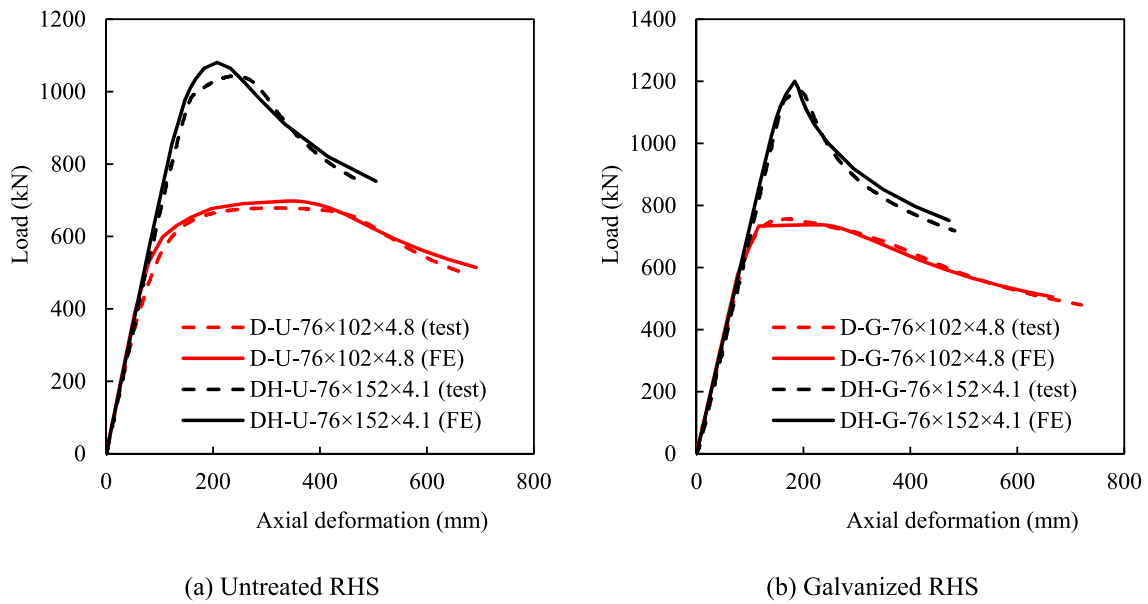


Fig. 7. Comparison of load-displacement relationships.

best fit line, the normalized plate slenderness ratio ($\bar{\lambda}$) corresponding to a P_u/P_y -ratio of one is often considered as the slenderness limit. For the indirect-formed SHS in Fig. 9, instead of a linear regression of the scatter, it is logical and conservative to consider the lower bound of the data. Nevertheless, based on the available data in Fig. 9, the slenderness

limit suitable for the direct-formed SHS can be larger than that of the indirect-formed SHS, due to the inherently low level of residual stress as a result of the direct forming approach. The untreated direct-formed SHS and the hot-finished SHS are compared in Fig. 10. It should be noted that the hot-finished SHS are typically heated to a normalizing

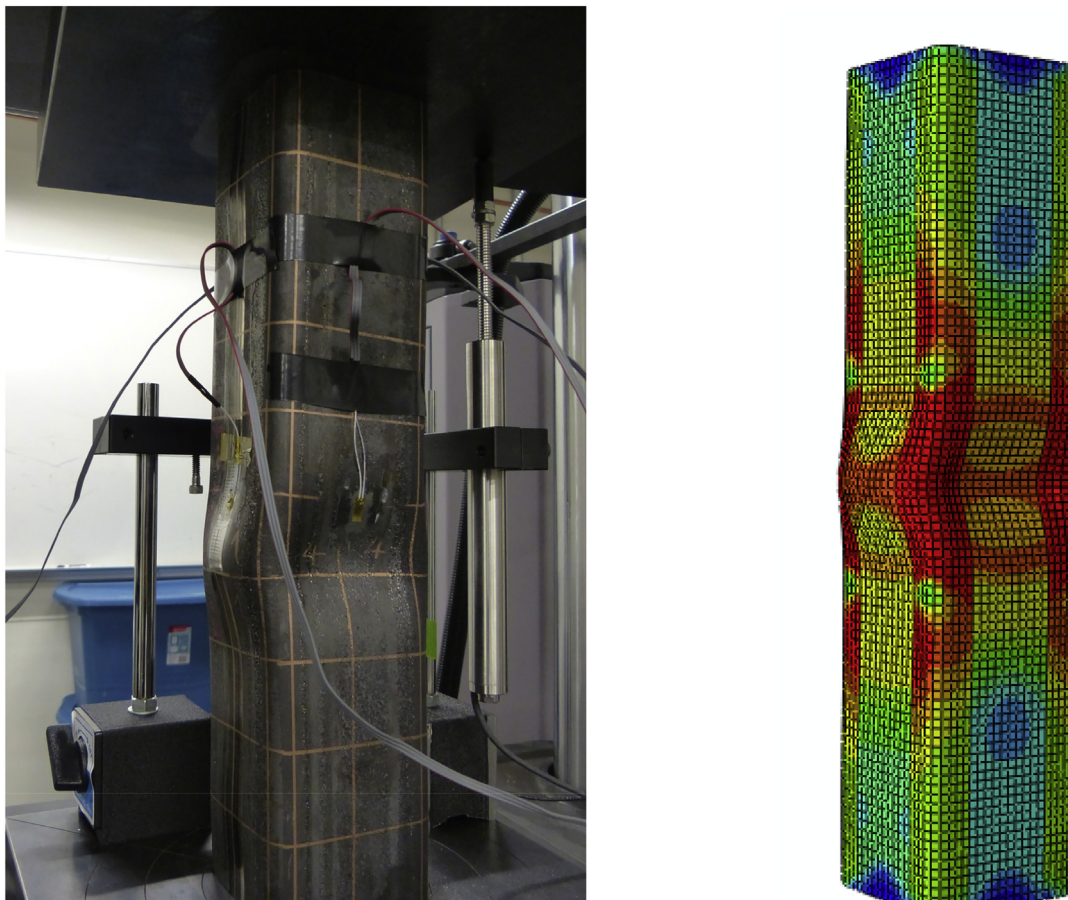


Fig. 8. Comparison of failure modes.

Table 4
Comparison of ultimate loads for direct-formed regular-strength SHS/RHS.

Specimen ID	P_{test} (kN)	Maximum local geometric imperfection	
		0.12 t	0.023 α
		P_{FE}/P_{test}	P_{FE}/P_{test}
D-U-76 × 102 × 3.2	459	0.89	0.88
D-G-76 × 102 × 3.2	507	0.95	0.94
D-U-76 × 102 × 4.8	679	0.99	1.01
D-G-76 × 102 × 4.8	757	0.96	0.97
D-U-102 × 102 × 3.2	478	0.93	0.92
D-G-102 × 102 × 3.2	539	0.97	0.96
D-U-102 × 102 × 4.8	839	0.93	0.96
D-G-102 × 102 × 4.8	913	0.93	0.94
D-U-127 × 127 × 4.8	969	0.89	0.91
D-G-127 × 127 × 4.8	1091	0.92	0.94
Mean		0.94	0.94
COV		0.033	0.035

Table 5
Comparison of ultimate loads for direct-formed high-strength SHS/RHS.

Specimen ID	P_{test} (kN)	Maximum local geometric imperfection	
		0.12 t	0.023 α
		P_{FE}/P_{test}	P_{FE}/P_{test}
DH-U-76 × 76 × 4.8	1116	0.96	0.97
DH-G-76 × 76 × 4.8	1100	0.97	0.97
DH-U-76 × 102 × 3.2	666	0.97	0.91
DH-U-76 × 102 × 3.2 ^a	678	0.95	0.90
DH-G-76 × 102 × 3.2	773	0.92	0.86
DH-G-76 × 102 × 3.2 ^a	784	0.91	0.85
DH-U-76 × 102 × 4.1	1052	0.96	0.92
DH-G-76 × 102 × 4.1	1109	0.95	0.91
DH-U-76 × 102 × 4.8	1276	0.98	0.98
DH-G-76 × 102 × 4.8	1241	1.02	1.02
DH-U-76 × 152 × 4.1	1043	1.02	0.99
DH-U-76 × 152 × 4.1 ^a	1052	1.01	0.98
DH-G-76 × 152 × 4.1	1169	0.99	0.95
DH-G-76 × 152 × 4.1 ^a	1189	0.97	0.94
Mean		0.97	0.94
COV		0.033	0.051

^a indicates a repeated test.

temperature of approximately 900 °C for a fine and homogeneous grain structure. This process improves material toughness and relieves residual stress. However, heat treatment at such temperature removes the strength enhancement from cold forming. Clear trade-offs between material strength and residual stress have been found in previous research [8,9] by comparing cold-formed hollow section materials heat-treated to 595 °C to their untreated counterparts. For a similar reason, the hot-finished SHS in many cases have lower P_u/P_y -ratios than the untreated direct-formed SHS in Fig. 10. In all, the direct-formed SHS exhibited superior stub column capacities over a wide range of cross-section slenderness.

Based on the experimental data from a limited number of hollow section specimens in the complimentary research [8,9], it was concluded that the application of hot-dip galvanizing in many cases increased stub column capacity and delayed local buckling, and in some cases, converted slender cross sections to non-slender cross sections. By performing a comprehensive parametric study in this research, such observation is confirmed by the comparisons in Figs. 11 and 12. As shown, the application of hot-dip galvanizing increased the P_u/P_y -ratios over a wide range of cross-section slenderness. Also shown in many cases in the figures are the conversions from slender to non-slender behaviour after galvanizing, as galvanizing reduces residual stress and delay local buckling.

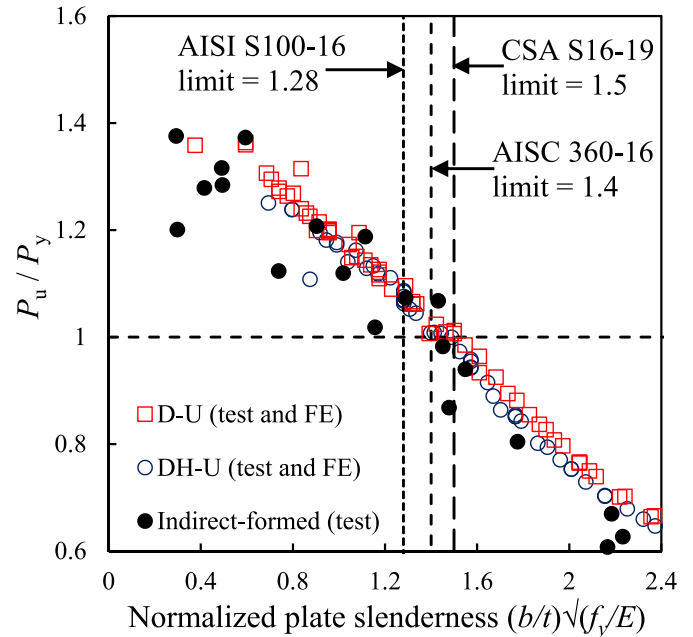


Fig. 9. Comparison of direct-formed SHS and indirect-formed SHS from [3,4,29,30].

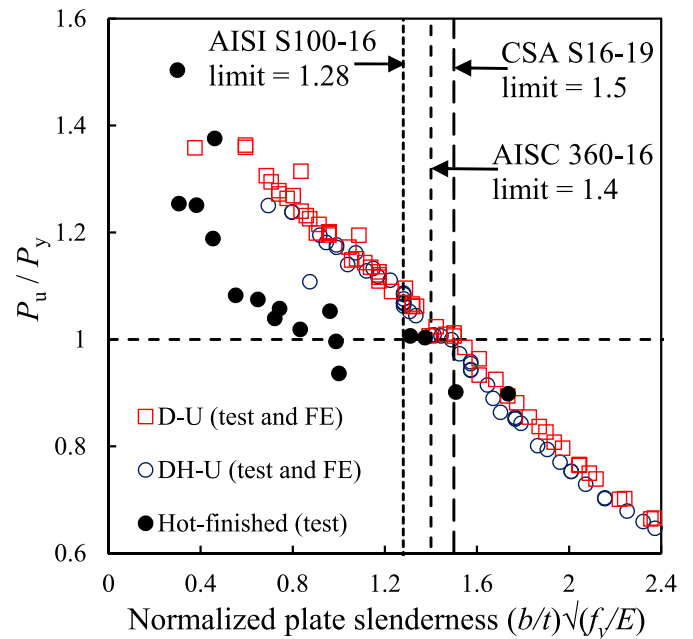


Fig. 10. Comparison of direct-formed SHS and hot-finished SHS from [4,29,31].

4. Evaluation of effective width method in AISC 360 and CSA S16

For the design of SHS/RHS members under axial compression using AISC 360-16 [15] and CSA S16-19 [12], cross-section classification is a critical procedure, where the width-to-thickness ratio of each plate element is evaluated against the slenderness limit individually. For SHS/RHS members with slender elements, AISC 360-16 [15] and CSA S16-19 [12] use the effective width method, which calculates the effective area of each plate element individually. In other words, this approach does not consider the entire cross-section directly, and the same methodology is applied to SHS and RHS. In this section, all 624 stub column models (312 SHS and 312 RHS) are used to evaluate the effective

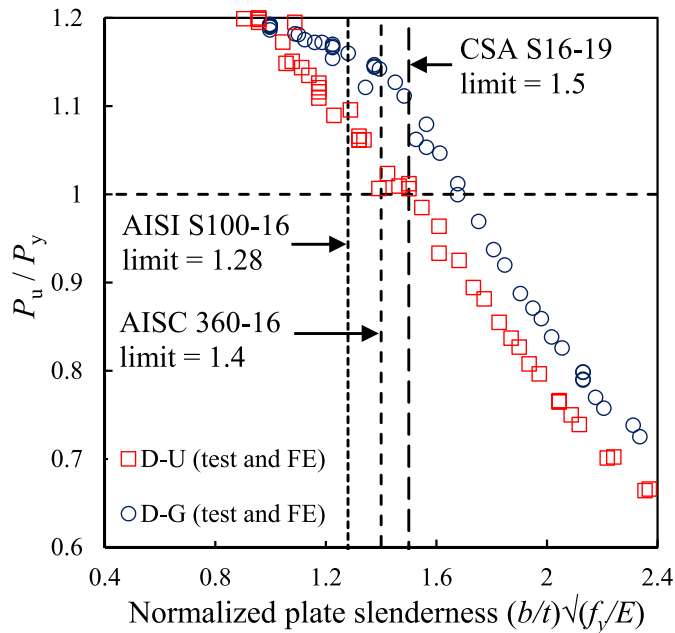


Fig. 11. Comparison of untreated and galvanized regular-strength direct-formed SHS.

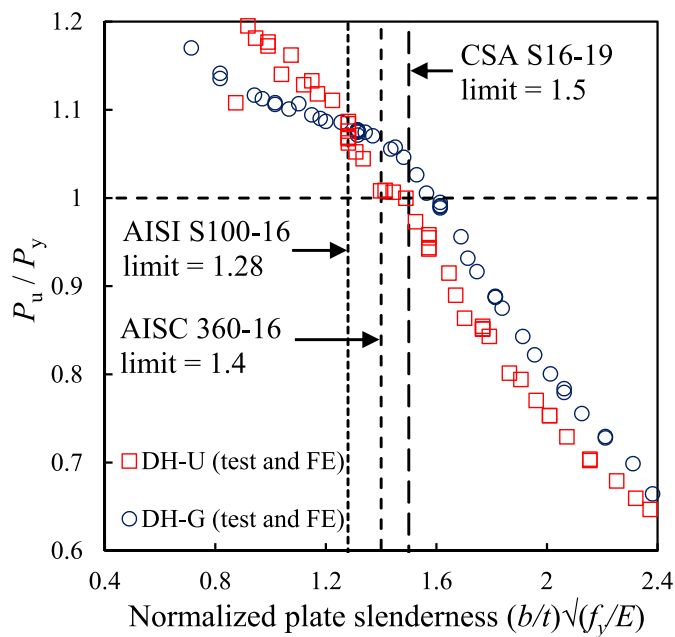


Fig. 12. Comparison of the untreated and galvanized high-strength direct-formed SHS.

width method in AISC 360-16 [15] and CSA S16-19 [12]. However, for clarity, only the SHS data is used in the figures in this section for graphical examination of the slenderness limits. This is consistent with the approach adopted by [4,6].

4.1. Cross-section classification

For the design of SHS/RHS under axial compression, members can be classified as cross sections without slender elements (i.e. nonslender) or cross sections with slender elements (i.e. slender). Slender sections under axial compression will experience local buckling before reaching the squash load. The yield slenderness limits in CSA S16-19 [12], AISC

360-16 [15] and AISI S100-16 [17] (based on the effective width method) are developed based on the elastic critical local buckling stress of a plate element under compression. A detailed discussion of this topic can be found in [8]. It should be noted that the existing cross-section classification and column design rules in various steel design standards do not differentiate SHS/RHS produced by different cold-forming methods. On the other hand, the experimental and numerical research evidence in the previous sections showed that: (1) the application of post-cold-forming hot-dip galvanizing can effectively reduce residual stress and, in return, improve stub column behaviour; and (2) direct-formed SHS/RHS in many cases exhibit better stub column behaviours than their indirect-formed and hot-finished counterparts. Therefore, the applicability of the existing cross-section classification rules to untreated and galvanized direct-formed SHS/RHS (regular- and high-strengths) needs to be evaluated individually.

To ensure that the comparisons are made based on the same criteria, the limiting width-to-thickness ratios for SHS/RHS plate elements from the three design standards are converted to the normalized yield slenderness limits ($\bar{\lambda}_{lim}$) in Table 6, using Eq. (8). A clear disparity among the selected design standards can be observed, as the $\bar{\lambda}_{lim}$ -values range from 1.28 to 1.50. The normalized yield slenderness limits are shown in Figs. 9–12 and are evaluated against the experimental and numerical data for direct-formed SHS/RHS from this study. It should be noted that the yield slenderness limit in EN 1993-1-1 [16] corresponds to a $\bar{\lambda}_{lim}$ -value of 1.405, which is similar to AISC 360-16 [15]. Therefore, EN 1993-1-1 [16] and the other design standards with similar limits are not included in the comparisons in Table 6 and Figs. 9–12. The slenderness limit from AISI S100-16 [17] (based on the effective width method) has been proven very conservative for cold-formed SHS/RHS in previous studies [4,6,8]. Therefore, only the slenderness limits in AISC 360-16 [15] and CSA S16-19 [12] will be further evaluated in this section.

As discussed earlier, to differentiate non-slender and slender cross-sections, previous research [e.g. 4,6,8] often consider the normalized plate slenderness ratio ($\bar{\lambda}$) corresponding to a P_u/P_y -ratio of one as the slenderness limit ($\bar{\lambda}_{lim}$). Following the same approach, based on the data in Figs. 11 and 12, the CSA S16-19 slenderness limit ($\bar{\lambda}_{lim} = 1.50$) is appropriate for the untreated direct-formed SHS (regular- and high-strength), while the AISC 360-16 limit ($\bar{\lambda}_{lim} = 1.40$) is conservative. On the other hand, slenderness limits of $\bar{\lambda}_{lim} = 1.70$ and 1.60 were observed from Figs. 11 and 12 for galvanized regular-strength SHS and galvanized high-strength SHS, respectively. Therefore, a $\bar{\lambda}_{lim}$ -value of 1.60 can be conservatively assigned to galvanized SHS (regular- and high-strength). For a more accurate evaluation of proposed yield slenderness limits, reliability analyses are performed in Section 5.

4.2. Cross-sectional capacity

In AISC 360-16 [15] and CSA S16-19 [12], the squash load is used as the nominal stub column strength for members without slender plate elements. For members with slender plate elements, the effective area is determined by deducting from the gross area, the ineffective area calculated as $(b - b_e)/t$, where b_e is the effective width of the plate element. The nominal stub column strength, in this case, is the product of the effective area and yield stress.

For all SHS/RHS specimens and FE models, following the design rules in AISC 360-16 [15] and CSA S16-19 [12], the nominal compressive strengths (P_n) (i.e., resistance factor = 1.0) are calculated. The nominal compressive strengths are then normalized by the cross-sectional squash loads (P_y). Using the normalized nominal strengths, the AISC and CSA design curves for the SHS specimens and FE models are plotted in Figs. 13 and 14, respectively. The normalized ultimate loads (P_u / P_y) from experimental testing and FE analysis are also shown in Figs. 13 and 14 for comparison. The key statistics are listed in Table 7. The following observations can be made:

Table 6
Yield slenderness limits for SHS/RHS plate elements in existing standards.

Design standard	Normalized yield slenderness limit
CSA S16-19 [12]	$\bar{\lambda}_{lim} = 1.50$
ANSI/AISC 360-16 [15]	$\bar{\lambda}_{lim} = 1.40$
AISI S100-16 [17] based on the effective width method	$\bar{\lambda}_{lim} = 1.28$

- (1) As shown in Fig. 13, for SHS without slenderness elements, the AISC 360-16 approach provides very conservative predictions, since the strength enhancement due to cold forming is not considered.
- (2) As shown in Fig. 13, for untreated direct-formed SHS with slender elements, the AISC 360-16 approach provides

accurate predictions. On the other hand, this approach is conservative for galvanized direct-formed SHS with intermediate slenderness since the existing slenderness limit ($\bar{\lambda}_{lim} = 1.40$) is conservative. As a result, the effective width method based on the existing slenderness limits caused strength underestimation due to unnecessary penalties on the effective cross-sectional area.

- (3) It should be noted that Fig. 13 shows only the SHS data (i.e. the plate slenderness is the same for all four sides). For RHS with slender elements, very often the two shorter sides are “nonslender”. In other words, the two shorter sides usually have $P_u/P_y > 1.0$, while the squash load is used as the nominal design strength for them. Also different from SHS, for RHS the shorter sides provide relatively stronger resistance to the longer sides against local buckling. Therefore, comparing to SHS, the AISC 360-16 approach is more conservative for RHS.

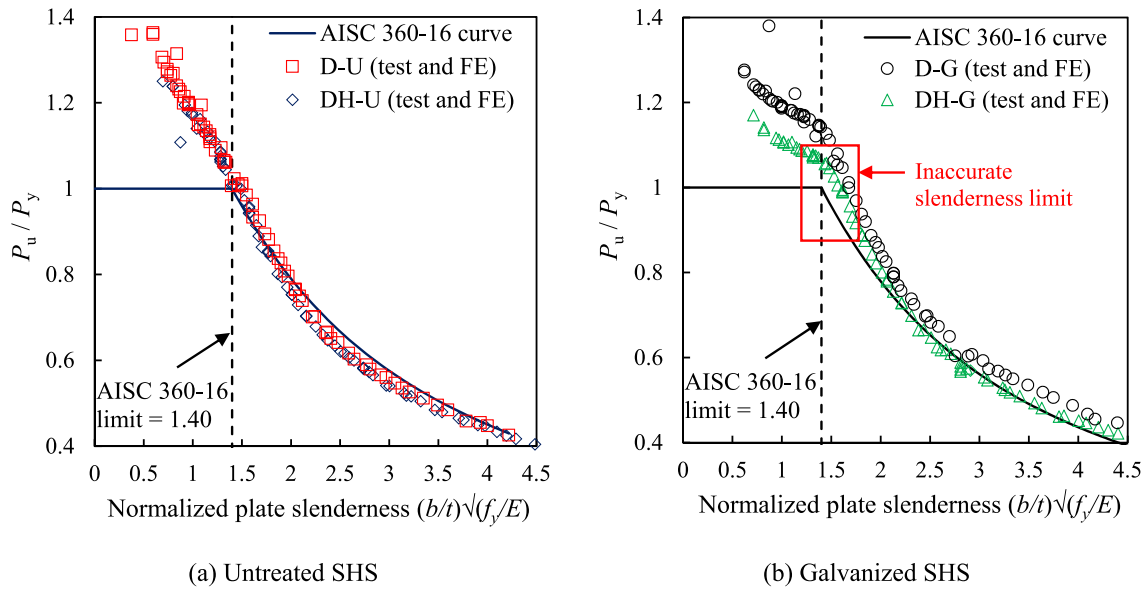


Fig. 13. Comparisons of SHS results with nominal strengths calculated using AISC 360-16 [15].

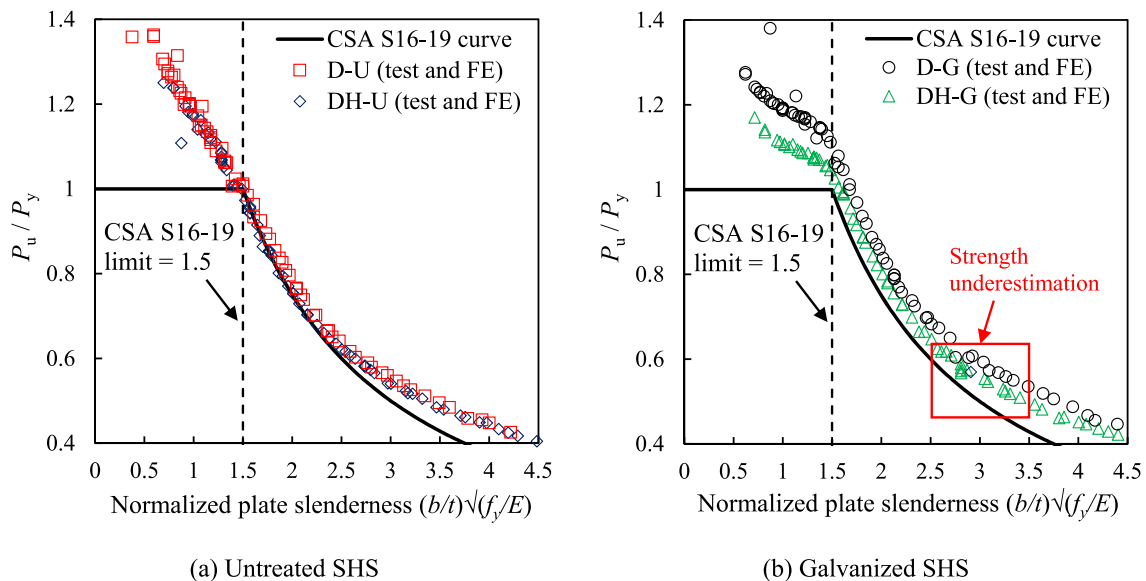


Fig. 14. Comparisons of SHS results with nominal strengths calculated using CSA S16-19 [12].

Table 7
Comparison of SHS/RHS test and FE results with design standard predictions.

Design standard	Untreated		Galvanized	
	$(P_u/P_n)_{mean}$	$(P_u/P_n)_{cov}$	$(P_u/P_n)_{mean}$	$(P_u/P_n)_{cov}$
CSA S16-19 [12]	1.10	0.084	1.14	0.054
AISC 360-16 [15]	1.07	0.107	1.10	0.074

- (4) For all SHS and RHS, the test and FE results are compared to the nominal design strengths calculated using the AISC 360-16 approach (calculated using the measured geometric and material properties). The key statistics are shown in Table 7. As shown, the AISC 360-16 approach is conservative when considering all SHS and RHS. However, the statistics do not reflect explicitly the different levels of conservativeness over the full range of normalized plate slenderness, especially for RHS (i.e. the four sides have different plate slenderness-values). Therefore, in Section 5, reliable analysis is performed for non-slender and slender sections individually.
- (5) As shown in Table 7, the CSA S16-19 approach is in general more conservative than the AISC 360-16 approach. As shown in Fig. 14, the CSA S16-19 approach is more accurate for sections with intermediate slenderness since it has a higher slenderness limit ($\bar{\lambda}_{lim} = 1.50$). However, this approach becomes inaccurate when the plate slenderness increases. Again, comparing to SHS, the effective width method in CSA S16-19 becomes even more conservative for RHS.
- (6) Overall, the AISC 360-16 approach in general gives better predictions. Therefore, only the AISC 360-16 approach will be further studied and modified in Section 5.

5. Design recommendations based on the effective width method

5.1. Modified approach based on AISC 360

As discussed earlier, comparing to CSA S16-19 [12], the existing formula in AISC 360-16 [15] gives better predictions of the experimental and FE results over a wide range of normalized plate slenderness. Therefore, the existing design rules in AISC 360-16 [15] are used in this section to develop the modified effective width method (MEWM) for the stub column design of untreated and galvanized direct-formed SHS/RHS.

In AISC 360-16 [15], for the design of SHS/RHS members under compression, the limit states include flexural buckling and local buckling. For SHS/RHS members without slender element, the nominal compressive strength (P_n) (based on the limit state of flexural buckling) is the product of the gross cross-sectional area and the critical stress. On the other hand, for SHS/RHS members with slender elements, the nominal compressive strength (P_n) (based on the limit state of flexural buckling and local buckling) is the product of the effective cross-sectional area and the critical stress. For stub columns (with or without slender element), the critical stress approximately equals the yield stress.

For SHS/RHS members with slender elements, the total effective cross-sectional area is the sum of corner areas and the effective flat face areas. The corner areas are calculated, assuming an outer corner radius of two times the wall thickness. The effective flat face areas are calculated by multiplying the wall thickness by the effective plate element widths (b_e). The current approach in AISC 360-16 [15] for calculation of the effective width of plate elements in SHS/RHS stub columns (i.e., critical stress = yield stress) is reproduced herein as Eq. (9).

$$\frac{b_e}{b} = \begin{cases} 1 & \bar{\lambda} \leq \bar{\lambda}_{lim} \\ \left[1 - c_1 \left(\frac{c_2 \bar{\lambda}_{lim}}{\bar{\lambda}} \right) \right] \cdot \left(\frac{c_2 \bar{\lambda}_{lim}}{\bar{\lambda}} \right) & \bar{\lambda} > \bar{\lambda}_{lim} \end{cases} \quad (9)$$

where $\bar{\lambda} = (b/t) \sqrt{f_y/E}$ (i.e. Eq. (8)); c_1 and c_2 are effective width imperfection adjustment factors. For SHS/RHS members, the values of

$c_1 = 0.2$ and $c_2 = 1.38$ are proposed in AISC 360-16 [15]. As shown in Table 6, for plate elements in SHS/RHS members under axial compression, a $\bar{\lambda}_{lim}$ -value of 1.40 is currently used in AISC 360-16 [15].

Based on the evidence in Sections 3 and 4, this research proposes a modified effective width method (MEWM) which uses of a $\bar{\lambda}_{lim}$ -value of 1.50 for untreated direct-formed SHS/RHS, and a $\bar{\lambda}_{lim}$ -value of 1.60 for galvanized direct-formed SHS/RHS. To be consistent with the existing plate element classification formula in Table B4.1a of AISC 360-16 [15], the new formulae corresponding to the proposed $\bar{\lambda}_{lim}$ -values are listed in Table 8. The proposed slenderness limits apply to direct-formed SHS/RHS with nominal yield stresses of 350 and 690 MPa. Using the proposed slenderness limits together with the existing AISC 360-16 design rules [15], the nominal compressive strengths (P_n) (i.e. resistance factor = 1.0) are calculated. The nominal compressive strengths are compared to all SHS/RHS test and FE results. For untreated direct-formed SHS/RHS, the mean of the P_u / P_n -ratio is 1.05, with a COV of 0.127. For galvanized direct-formed SHS [D-G and DH-G in Fig. 14(b)], the mean of the P_u / P_n -ratio is 1.05, with a COV of 0.111.

5.2. Reliability analysis of the modified approach based on AISC 360

To evaluate whether the modifications proposed in Section 5.1 (to the existing AISC 360-16 design rules [15]) provide adequate or excessive safety margins over different ranges of plate slenderness, reliability analyses were conducted considering a target reliability index of 2.6 recommended by AISC 360-16 [15]. The load combination used in the reliability analysis follows [15] (i.e., a load combination of 1.2DL + 1.6LL and a LL-over-DL-ratio of three, where LL = live load and DL = dead load). For the design of members under axial compression, AISC 360-16 [15] uses a resistance factor (ϕ) of 0.9.

The AISI S100-16 [17] formula (reproduced as Eq. (10) herein) was used to calculate the reliability index (β). It should be noted that Eq. (10) is the same as the reliability index formula in Commentary Chapter B of AISC 360-16 [15]. The later can be derived using the specified load combination and LL-over-DL ratio. The definitions of the parameters in Eq. (10) are included in ‘‘Nomenclatures.’’ The parameters were calculated using the experimental and FE data in this study and are listed in Table 9.

$$\beta = \frac{\ln \left(\frac{C_\phi \cdot M_m \cdot F_m \cdot P_m}{\phi} \right)}{\sqrt{V_M^2 + V_F^2 + V_P^2 + V_Q^2}} \quad (10)$$

Using the parameters listed in Table 9, reliability analyses were performed on the proposed modified effective width method (MEWM) for stub column design of untreated direct-formed SHS/RHS ($\bar{\lambda}_{lim} = 1.50$) and galvanized direct-formed SHS/RHS ($\bar{\lambda}_{lim} = 1.60$). The calculated β -values are listed in Table 10. The following observations can be made:

- (1) When considering, from the experimental and FE data pool, only the SHS/RHS with slender elements, for a resistance factor of 0.90, the reliability indices for untreated sections and galvanized sections are 2.60 and 2.84, respectively. Both reliability indices are no less than the target value of 2.6 recommended by AISC

Table 8
Proposed yield slenderness limits for direct-formed SHS/RHS plate elements.

Design standard	Proposed normalized yield slenderness limit	Corresponding formula
ANSI/AISC 360-16 [15]	Untreated: $\lambda_{lim} = 1.50$	$b/t \leq 1.50 \sqrt{E/f_y}$
	Galvanized: $\lambda_{lim} = 1.60$	$b/t \leq 1.60 \sqrt{E/f_y}$

Table 9
Parameters for calculation of reliability indices for modified effective width method (MEWM).

	Untreated			Galvanized		
	Nonslender Sections	Slender Sections	Nonslender + Slender Sections	Nonslender Sections	Slender Sections	Nonslender + Slender Sections
C_ϕ	1.49	1.49	1.49	1.49	1.49	1.49
M_m	1.07	1.07	1.07	1.14	1.14	1.14
F_m	1.03	1.03	1.03	1.03	1.03	1.03
P_m	1.18	0.95	1.05	1.16	0.97	1.05
V_M	0.087	0.087	0.087	0.089	0.089	0.089
V_F	0.030	0.030	0.030	0.030	0.030	0.030
V_P	0.077	0.057	0.127	0.054	0.080	0.111
V_Q	0.187	0.187	0.187	0.187	0.187	0.187

360-16 [15]. Therefore, adequate safety margins are inherent in the proposed modified effective width method (MEWM) for sections with slender elements.

- (2) When considering only the SHS/RHS without slender elements, for a resistance factor of 0.90, the reliability indices for untreated sections and galvanized sections are 3.48 and 3.77, respectively. The values are much larger than 2.6. This indicates an excessive safety margins since, as discussed earlier, the effective width method uses the squash load as the nominal stub column strength of sections without slender elements (i.e. does not account for the strength enhancement due to cold forming).
- (3) Based on the experimental and FE data from all SHS/RHS (i.e. sections with and without slender elements), for a resistance factor of 0.90, the reliability indices for untreated sections and galvanized sections are 2.69 and 3.02, respectively. Both reliability indices are larger than the target value of 2.6 recommended by AISI 360-16 [15]. Therefore, the proposed modified effective width method (MEWM) is overall reliable.

6. Design recommendations based on the direct strength method

6.1. Modified approach based on AISI S100

As discussed in Section 5, for cross sections without slender elements, the effective width method in AISI 360-16 [15] and CSA S16-19 [12] use the squash load (P_y) as the nominal stub column strength. Therefore, for cross sections with small slenderness ratios, the nominal stub column strengths are significantly lower than the actual ultimate loading capacities (P_u from experimental testing and FE analysis), since the strength enhancement due to cold forming is ignored. This is consistent with the findings in [3,6]. In order to fully appreciate the advantage of untreated and galvanized direct-formed RHS (i.e. low overall level of residual stress and strength enhancement due to cold forming), a modified direct strength method (MDSM) based on AISI S100-16 [17] is proposed in this section, using the experimental and FE results of all SHS and RHS.

As discussed previously, the effective width method calculates the member strength based on the evaluation of individual plate elements. On the other hand, the direct strength method (DSM) in AISI

Table 10
Reliability indices calculated based on modified effective width method (MEWM).

Material Type	Nonslender		Slender		Nonslender + Slender	
	ϕ	β	ϕ	β	ϕ	β
Untreated (D-U + DH-U)	0.9	3.48	0.9	2.60	0.9	2.69
Galvanized (D-G + DH-G)	0.9	3.77	0.9	2.84	0.9	3.02

S100-16 [17] is based on the behaviour of the entire cross section, where inter-element compatibility and equilibrium are considered [32,33]. For sections with slender elements under compression and flexure, the direct strength method (DSM) in AISI S100-16 [17] does not involve calculation of effective area and effective section modulus. Therefore, it is particularly efficient for thin-walled cold-formed steel structural members. The existing DSM formula from AISI S100-16 [17] for calculation of nominal compressive strength involving local buckling is reproduced here in as Eq. (11).

$$\frac{P_{nl}}{P_{ne}} = \begin{cases} 1 & \lambda_l \leq 0.776 \\ \left[1 - 0.15 \left(\frac{1}{\lambda_l} \right)^{0.8} \right] \cdot \left(\frac{1}{\lambda_l} \right)^{0.8} & \lambda_l > 0.776 \end{cases} \quad (11)$$

where P_{nl} = nominal compressive strength for local buckling; P_{ne} = global column strength; $\lambda_l = \sqrt{P_{ne}/P_{cr1}}$ = slenderness factor; and P_{cr1} = critical elastic local column buckling load.

For all direct-formed SHS/RHS stub column specimens and FE models, P_{ne} is determined by multiplying the gross section area by f_y . Following the recommendation in AISI S100-16 [17], P_{cr1} is obtained by conducting a finite strip analysis using the CUFSM software [33]. Following this approach, the DSM design curves are obtained, and are shown in Fig. 16a and b for untreated and galvanized sections, respectively.

The experimental and numerical ultimate strengths of the stub columns are normalized by the cross-sectional squash loads (P_y). The normalized values are plotted against $\sqrt{P_{ne}/P_{cr1}}$ in Fig. 15 for comparison. The following observations can be made:

- (1) Similar to the effective width method, the existing DSM is very conservative for sections with slenderness factor (λ_l) below the threshold (0.776).
- (2) Comparing to untreated SHS/RHS, DSM is more conservative for galvanized SHS/RHS.

To consider the cold-forming-induced strength enhancement and the effect of hot-dip galvanizing, based on nonlinear least squares regressions, Eqs. (12) and (13) are proposed in this study for untreated and galvanized direct-formed SHS/RHS. The formulae can be used to determine the local-to-global buckling strength ratio (P_{nl}/P_{ne}).

For untreated direct-formed SHS/RHS with regular- and high-strength:

$$\frac{P_{nl}}{P_{ne}} = \begin{cases} - \left[1 - 0.13 \left(\frac{1}{\lambda} \right)^{0.9} \right] \left(\frac{1}{\lambda} \right)^{0.9} + 2 \quad (\lambda = -\lambda_l + 1.66 \text{ when } \lambda_l \leq 0.83) \\ \left[1 - 0.13 \left(\frac{1}{\lambda} \right)^{0.9} \right] \left(\frac{1}{\lambda} \right)^{0.9} \quad (\lambda = \lambda_l \text{ when } \lambda_l > 0.83) \end{cases} \quad (12)$$

For galvanized direct-formed SHS/RHS with regular- and high-strength:

$$\frac{P_{nl}}{P_{ne}} = \begin{cases} - \left[1 - 0.034 \left(\frac{1}{\lambda} \right)^{0.5} \right] \left(\frac{1}{\lambda} \right)^{0.5} + 2 \quad (\lambda = -\lambda_l + 1.86 \text{ when } \lambda_l \leq 0.93) \\ \left[1 - 0.059 \left(\frac{1}{\lambda} \right)^{0.9} \right] \left(\frac{1}{\lambda} \right)^{0.9} \quad (\lambda = \lambda_l \text{ when } \lambda_l > 0.93) \end{cases} \quad (13)$$

where λ = new slenderness factor based on λ_l in Eq. (11) from the direct strength method (DSM) in AISI S100-16 [17].

The nominal strength calculated using Eqs. (12) and (13) are compared to the experimental and FE data in Fig. 16a and b for untreated and galvanized direct-formed SHS/RHS, respectively. As shown, the proposed modified direct strength method (MDSM) formulae provide

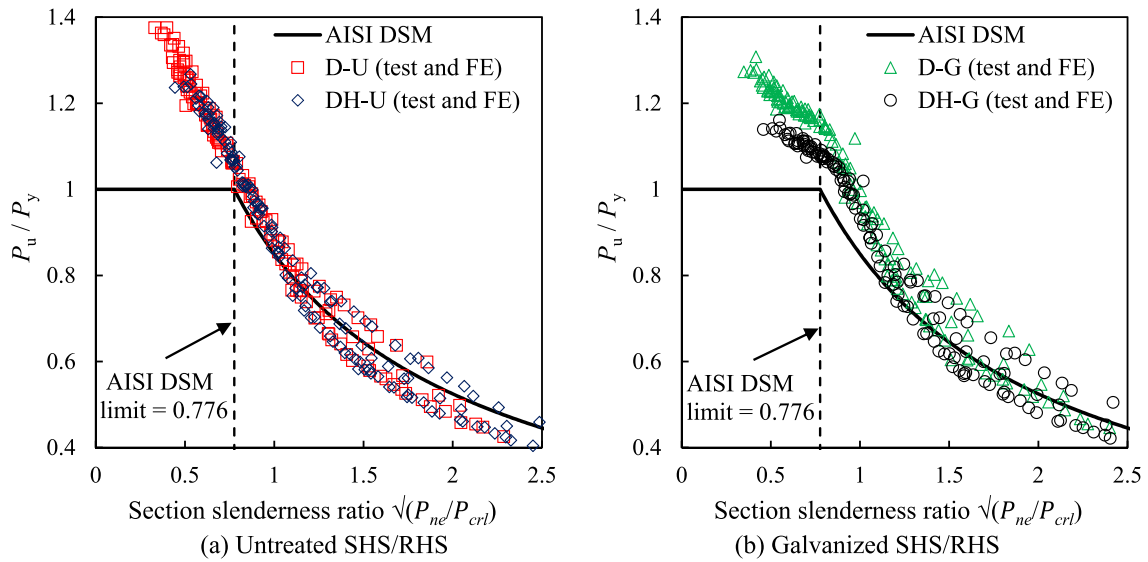


Fig. 15. Comparisons of SHS/RHS results with nominal strengths calculated using direct strength method in AISI S100-16 [17].

accurate predictions in both cases. To evaluate whether the proposed modifications provide adequate or excessive safety margins, a reliability analysis is performed in Section 6.2.

6.2. Reliability analysis on the modified approach based on AISI S100

Unlike the effective width method (e.g. Figs. 13 and 14), as shown in Fig. 16 the proposed MDSM generate a relatively uniform margin of safety for all SHS/RHS over the entire range of slenderness ratios. Therefore, in this section the reliability analyses for the untreated and galvanized SHS/RHS are performed using all experimental and FE data in each category. For design of members in compression, AISI S100-16 [17] adopts a resistance factor of 0.85. For reliability analysis, AISI S100-16 [17] uses a LL/DL-ratio of five, and a target reliability index of 2.5. Based on the approach discussed in Section 5.2, using the experimental and FE data, the parameters for use in Eq. (10) are calculated and listed in Table 11. The calculated reliability indices are listed in Table 12. As shown, for both untreated and

galvanized sections, the values are larger than the target reliability index of 2.5. Therefore, adequate safety margins are inherent in the proposed MDSM.

Table 11

Parameters for calculation of reliability indices for modified direct strength method (MDSM).

	Untreated	Galvanized
	Nonslender + Slender Sections	Nonslender + Slender Sections
C_ϕ	1.52	1.52
M_m	1.07	1.14
F_m	1.03	1.03
P_m	1.01	1.02
V_M	0.087	0.089
V_F	0.030	0.030
V_P	0.046	0.055
V_Q	0.21	0.21

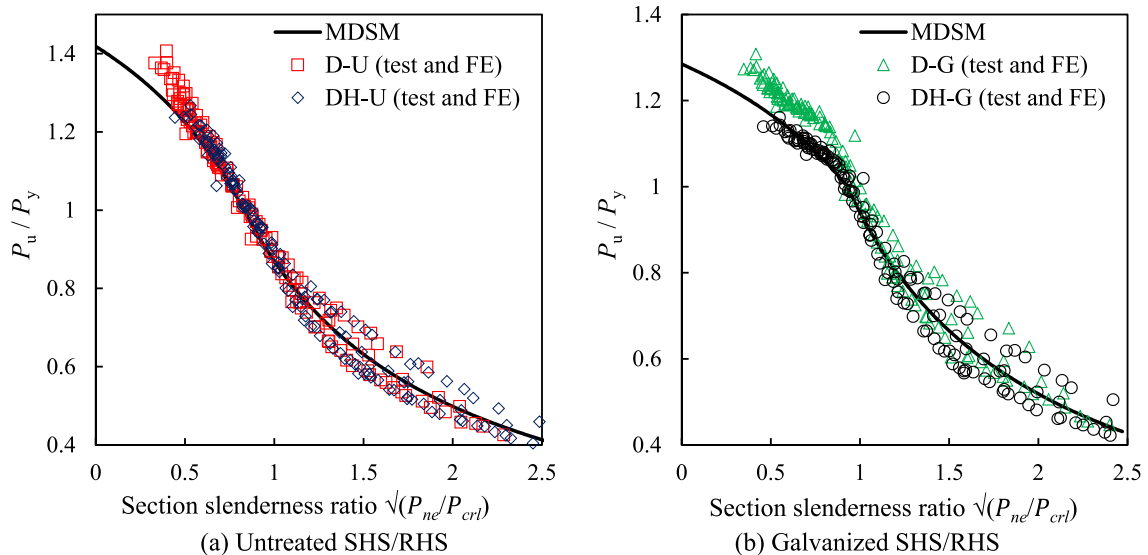


Fig. 16. Comparisons of SHS/RHS results with nominal strengths calculated using modified direct strength method (MDSM).

Table 12
Reliability indices calculated based on modified direct strength method (MDSM).

Material type	Nonslender + Slender	
	ϕ	β
Untreated (D-U + DH-U)	0.85	2.97
Galvanized (D-G + DH-G)	0.85	3.23

7. Conclusions

This paper presents a comprehensive research on the effects of direct-forming and post-production hot-dip galvanizing on the stub column behaviour of cold-formed SHS/RHS. A total of 624 FE models were developed using the previously measured residual stresses, strength properties and geometric imperfections in direct-formed SHS/RHS. The FE modelling approach was validated against previous experimental data from 24 stub column tests. Both the stub column specimens and FE models cover wide ranges of geometric and material strength properties. By comparing to the stub column test results from previous studies for indirect-formed and hot-finished SHS/RHS, it was found that: (1) direct-formed SHS/RHS have superior stub column behaviour; and (2) the application of post-production galvanizing can effectively improve the stub column behaviour by relieving the residual stress. Based on the research evidence, the effective width method in AISC 360-16 [15] and CSA S16-19 [12], and the direct strength method in AISI S100-16 [17] were found to be conservative for both untreated and galvanized direct-formed SHS/RHS. Modified effective width method (MEWM) and modified direct strength method (MDSM) are proposed. The proposed modifications were proven accurate based on reliability analyses.

Author Statement

The work has not been published previously. It is not under consideration for publication elsewhere. The publication is approved by all authors. If accepted, it will not be published elsewhere in the same form, in English or in any other language, including electronically without the written consent of the copyright-holder.

Declaration of Competing Interest

The authors declare that they have no known competing financial interests or personal relationships that could have appeared to influence the work reported in this paper.

Acknowledgements

Financial support has been provided by the Natural Sciences and Engineering Research Council of Canada (NSERC), the Canadian Institute of Steel Construction (CISC). Appreciation is extended to Bull Moose Tube and Silver City Galvanizing for their donation of material and service.

References

- [1] X.-L. Zhao, A. Heidarpour, L. Gardner, Recent developments in high-strength and stainless steel tubular members and connections, *Steel Constr.* 7 (2014) 65–72.
- [2] T.M. Chan, X.L. Zhao, B. Young, Cross-section classification for cold-formed and built-up high strength carbon and stainless steel tubes under compression, *J. Constr. Steel Res.* 106 (2015) 289–295.
- [3] J.L. Ma, T.M. Chan, B. Young, Experimental investigation on stub-column behavior of cold-formed high-strength steel tubular sections, *J. Struct. Eng.* 142 (2016), 04015174.
- [4] J. Wang, S. Afshan, N. Schillo, M. Theofanous, M. Feldmann, L. Gardner, Material properties and compressive local buckling response of high strength steel square and rectangular hollow sections, *Eng. Struct.* 130 (2017) 297–315.
- [5] B. Somodi, B. Kövesdi, Flexural buckling resistance of cold-formed HSS hollow section members, *J. Constr. Steel Res.* 128 (2017) 179–192.
- [6] J.L. Ma, T.M. Chan, B. Young, Design of cold-formed high-strength steel tubular stub columns, *J. Struct. Eng.* 144 (2018), 04018063.
- [7] X. Lan, J. Chen, T.M. Chan, B. Young, The continuous strength method for the design of high strength steel tubular sections in compression, *Eng. Struct.* 162 (2018) 177–187.
- [8] K. Tayyebi, M. Sun, Stub column behaviour of heat-treated and galvanized RHS manufactured by different methods, *J. Constr. Steel Res.* 166 (2020) 105910.
- [9] K. Tayyebi, M. Sun, K. Karimi, Residual stresses of heat-treated and hot-dip galvanized RHS cold-formed by different methods, *J. Constr. Steel Res.* 169 (2020) 106071.
- [10] CSA, General requirements for rolled or welded structural quality steel / Structural quality steel, CSA G40.20-13/G40.21-13, Canadian Standards Association, Toronto, Canada, 2013.
- [11] ASTM, Standard specification for cold-formed welded carbon steel hollow structural sections (HSS), ASTM A1085/A1085M-15, American Society for Testing and Materials, West Conshohocken, PA, USA, 2015.
- [12] CSA, Limit states design in structural steel, CSA S16-19, Canadian Standard Association, Toronto, ON, Canada, 2019.
- [13] M. Sun, J.A. Packer, Hot-dip galvanizing of cold-formed steel hollow sections: a state-of-the-art review, *Front. Struct. Civ. Eng.* 13 (2019) 49–65.
- [14] M. Sun, Z. Ma, Effects of heat-treatment and hot-dip galvanizing on mechanical properties of RHS, *J. Constr. Steel Res.* 153 (2019) 603–617.
- [15] ANSI/AISC, Specification for structural steel buildings, ANSI/AISC 360-16, Chicago, IL, USA, 2016.
- [16] CEN, Eurocode 3—design of steel structures—Part 1-1: General rules and rules for buildings, BS EN-1993-1-1, British Standards Institution, London, UK, 2005.
- [17] AISI, North American Specification for the Design of Cold-Formed Steel Structural Members, AISI S100-16, American Iron and Steel Institute, Washington, DC, 2016.
- [18] ABAQUS, Dassault Systèmes, ABAQUS Version 6.14 [Computer software], 2014.
- [19] X. Yun, L. Gardner, Stress-strain curves for hot-rolled steels, *J. Constr. Steel Res.* 133 (2017) 36–46.
- [20] L. Gardner, X. Yun, Description of stress-strain curves for cold-formed steels, *Constr. Build. Mater.* 189 (2018) 527–538.
- [21] M. Ashraf, L. Gardner, D.A. Nethercot, Finite element modelling of structural stainless steel cross-sections, *Thin-Walled Struct.* 44 (10) (2006) 1048–1062.
- [22] B.W. Schafer, T. Peköz, Computational modeling of cold-formed steel: Characterizing geometric imperfections and residual stresses, *J. Constr. Steel Res.* 47 (1998) 193–210.
- [23] H.X. Yuan, Y.Q. Wang, Y.J. Shi, L. Gardner, Residual stress distributions in welded stainless steel sections, *Thin-Walled Struct.* 79 (2014) 38–51.
- [24] R.B. Cruise, L. Gardner, Residual stress analysis of structural stainless steel sections, *J. Constr. Steel Res.* 64 (3) (2008) 352–366.
- [25] J.L. Ma, T.M. Chan, B. Young, Material properties and residual stresses of cold-formed high strength steel hollow sections, *J. Constr. Steel Res.* 109 (2015) 152–165.
- [26] B. Somodi, B. Kövesdi, Residual stress measurements on cold-formed HSS hollow section columns, *J. Constr. Steel Res.* 128 (2017) 706–720.
- [27] M. Sun, J.A. Packer, Direct-formed and continuous-formed rectangular hollow sections — Comparison of static properties, *J. Constr. Steel Res.* 92 (2014) 67–78.
- [28] R.D. Ziemian, Guide to Stability Design Criteria for Metal Structures, John Wiley & Sons, Hoboken, USA, 2010.
- [29] L. Gardner, N. Saari, F. Wang, Comparative experimental study of hot-rolled and cold-formed rectangular hollow sections, *Thin-Walled Struct.* 48 (2010) 495–507.
- [30] T.G. Singh, K.D. Singh, Structural performance of YSt-310 cold-formed tubular steel stub columns, *Thin-Walled Struct.* 121 (2017) 25–40.
- [31] X. Meng, L. Gardner, Testing of hot-finished high strength steel SHS and RHS under combined compression and bending, *Thin-Walled Struct.* 148 (2020) 106262.
- [32] B.W. Schafer, Review: The direct strength method of cold-formed steel member design, *J. Constr. Steel Res.* 64 (2008) 766–778.
- [33] B.W. Schafer, S. Ádány, Buckling analysis of cold-formed steel members using cufsm: conventional and constrained finite strip methods, *Eighteenth Int. Spec. Conf. Cold-Formed Steel Struct.* Orlando, FL, Citeseer, 2006.